Carbohydrate Polymers 98 (2013) 936–942

Contents lists available at SciVerse ScienceDirect

Carbohydrate Polymers

journal homepage: www.elsevier.com/locate/carbpol

Functional cell-laden alginate scaffolds consisting of core/shell struts for tissue regeneration

SeungHyun Ahn, HyeongJin Lee, GeunHyung Kim *

Department of Bio-Mechatronic Engineering, College of Biotechnology and Bioengineering, Sungkyunkwan University, Suwon, South Korea

ARTICLE INFO

Article history:
Received 27 April 2013
Received in revised form 4 June 2013
Accepted 3 July 2013
Available online 11 July 2013

Keywords:
Cell-printing
Alginate
Tissue regeneration
Bone

ABSTRACT

We report an innovative cell-dispensing process using a three-axis robot system coupled with a micro-core/shell nozzle and an aerosol cross-linking process to achieve controlled mechanical properties and high cell viability of porous cell-laden alginate scaffolds. The scaffolds were fabricated into layer-by-layer struts, which were used to design the pore structure. The struts consisted of a core/shell region; a low weight fraction of alginate and cells (MC3T3-E1) was injected in the shell region to efficiently exchange nutrients and metabolic wastes, while a high weight fraction of alginate without cells was deposited in the core region to improve the mechanical properties of the cell-laden scaffold. After 10 days of cell culture, the cell viability (95%) in the shell region improved significantly compared to 70% for the cells homogeneously distributed in the struts, and the mechanical properties were enhanced from 1.4 to 15.7 kPa. Stained nuclei and F-actin images showed that the laden cells proliferated well on the functional hydrogel scaffold after 20 days of cell culture, indicating that the cells concentrated in the shell region of the struts survived and increased their metabolic functions during several incubation periods compared to the standard cell-laden scaffold. This innovative cell-dispensing technique represents a promising fabrication tool for obtaining bottom-up scaffolds for various tissue regenerations.

1. Introduction

Three-dimensional (3D) scaffolds mimicking an extra-cellular matrix (ECM) can be used to successfully regenerate various tissues, because they provide a spatial environment in which cells can easily attach, proliferate, and differentiate (Langer & Vacanti, 1993; Moutos, Freed, & Guilak, 2007). 3D biocompatible and biodegradable scaffolds have been combined with a patient's cells, and the regenerated tissues have been implanted in the patient (Atala, Bauer, Soker, Yoo, & Retik, 2006). Since Langer and Vacanti (1993) first proposed the idea of tissue regeneration, tissue engineering has shown great potential as an alternative for patients waiting for organ transplantation.

Recently, scaffold fabrication for tissue engineering has advanced from "top-down" to "bottom-up" methods. Various techniques have been proposed for bottom-up fabrication to overcome disadvantages of top-down fabrication, such as low or non-uniform cell seeding efficiency resulting in non-homogenous proliferation of the cells and a lack of multiple tissue regeneration (Boland, Xu, Damon, & Cui, 2006). Typical bottom-up fabrication techniques, which use a layer-by-layer method to print a mixture of cross-linkable hydrogels and various cells, include laser-assisted bio-printing based on laser-induced forward transfer (Koch et al., 2012; Ovsianikov et al., 2011), cell-laden hydrogel modules using size-controlled micro-fluidic channels (Bruzewicz, Mcguigan, & Whitesides, 2008), micro-molding (Geckil, Xu, Zhang, Moon, & Demirci, 2010), and bio-dispensing of cell-laden hydrogels(Ahn, Lee, Bonassar, & Kim, 2012; Cohen, Malone, Lipson, & Bonassar, 2006). In addition, cell-sheet-stacking technology (Yang et al., 2009) is also considered a promising bottom-up method.

Bottom-up fabrication methods offer several advantages over top-down methods, including homogeneous cell distribution in the whole scaffold, controllable cell density, and multiple printed cell types in one scaffold using a one-step process. However, although the bottom-up approach has several advantages, there are still problems that need to be overcome. According to Catros et al. (2012), laser-assisted bio-printing and ink-jet printing cannot be used to construct macroscopic (i.e., cm^3) scaffolds due to the limited scale of the processes; moreover, printed bio-inks lack the mechanical properties required to maintain the 3D shape during the cell-culture period. Matsunaga, Morimoto, and Takeuchi (2011) reported that a large-scale microscopic tissue structure greater than 500 μm has not yet been developed for the cell-sheet process due to process limitations. In addition, cell sheets thicker than 100 μm cannot provide sufficient pathways for nutrient transport and waste removal, resulting in cell necrosis in the center of the sheet (Haraguchi et al., 2012). Gaetani et al. (2012) reported that

* Corresponding author at: 2066 Sebu-Ro, Jangan-Gu, Suwon-Si Gyeonggi-Do, South Korea. Tel.: +82 31 290 7828.
E-mail address: gkimbme@skku.edu (G. Kim).

0144-8617/$ – see front matter © 2013 Elsevier Ltd. All rights reserved.
http://dx.doi.org/10.1016/j.carbpol.2013.07.008

Table 1
Processing parameters for cell-laden alginate struts.

	Control strut	Core/shell strut
Nozzle size (μm)	310	Core: 500, Shell: 900
Nozzle speed (mm s^{-1})	15	15
Pneumatic pressure (kPa)	220 ± 10	Core: 270 ± 30, Shell: 130 ± 14
Strut size (μm)	829 ± 42	723 ± 36
$CaCl_2$ in the aerosol spraying process (wt%)	2	
$CaCl_2$ in the cross-linking process (wt%)	2	
Cross-linking time (min)	1	
$CaCl_2$ flow rate in the aerosol spraying process (mL min^{-1})	1.5 ± 0.2	
Cells (number per mL)	1.6×10^6	
Alginate solution (wt%)	3.5	Core: 6, Shell: 3.5

non-porous cell-laden scaffolds showed low cell viability, about 41% compared to porous scaffolds, for human cardiac-derived cardiomyocyte progenitor cells (hCMPCs) after 7 days of cell culture.

To overcome the limitations of bottom-up techniques, a molding method using various cell beads, including NIH 3T3 cells and human umbilical endothelial cells, have been proposed (Matsunaga, Morimoto, & Takeuchi, 2011). The molding method enables the design of macro-sized tissue construction (i.e., millimeter-thick tissues) by stacking a large number of cell-covered collagen microbeads (diameter, 100–300 μm).

Recently, we proposed a new cell-dispensing process coupled with an aerosol process to obtain highly porous cell-laden 3D structures. Using this method, we produced highly porous cell-laden scaffolds consisting of alginate and preosteoblast cells (MC3T3-E1) having a high initial cell viability of about 84% (Ahn et al., 2012a,b). The fabricated cell-laden alginate scaffolds (20 mm × 20 mm × 4.5 mm) had a homogeneous pore size (400–500 μm), 100% pore-interconnectivity, and uniform strut size (500–600 μm). After 5 days, the difference in the cell viability of the preosteoblasts for the cell-laden alginates with and without micro-pores was about 64% (Ahn et al., 2012a,b). Although the scaffolds were several millimeters thick, the highly porous cell-laden alginate scaffolds provided conditions that increased cell survival compared to non-porous scaffolds. However, the cell viability for the porous cell-laden alginate still decreased from the initial cell viability (75% compared to 86%) after 5 days of cell culture. We attributed this result to the thick block (500–600 μm) of the cell-laden alginate struts, which is a limitation of the extrusion process using a micro-sized nozzle. For the outer area (surface) of the struts, the embedded cells can easily receive nutrients and oxygen; however, for the core area, the cells cannot receive sufficient nutrients or oxygen. Also, the mechanical properties of the porous cell-laden scaffold were significantly reduced due to the high porosity of the cell-laden scaffold.

In this study, we designed a cell-embedded core (pure alginate)/shell (alginate with cells) scaffold using a micro-sized core/shell nozzle dispensing system coupled with an aerosol cross-linking process to effectively increase the cell viability of cell-laden scaffolds after long cell-culture periods and control the mechanical properties. This system enabled precise manipulation of the core/shell structure and control of the cell distribution of the cell-laden struts in the radial direction. To compare the feasibility of the core/shell scaffold with a standard cell-laden scaffold, the scaffolds were cultured for long periods (20 days) to observe the cell viability and various cellular activities. In addition, to improve the poor mechanical properties of the porous cell-laden alginate scaffold, the core region in the core/shell struts was filled with a high weight fraction of alginate solution. By applying this technique, we fabricated a functional cell-laden scaffold with significantly high cell viability and dramatically improved mechanical properties.

2. Experimental

2.1. Cells and materials

MC3T3-E1 cells were provided by Prof. Claudia Fischbach–Teschl (Cornell University, Ithaca, NY, USA). For routine cell maintenance, MC3T3-E1 mouse calvaria osteoblast cells were cultured and maintained in α-minimum essential medium (Life Science, USA) containing 10% fetal bovine serum (FBS, Sigma–Aldrich, St. Louis, MO, USA). Low-viscosity, high-G-content, nonmedical-grade LF10/60 alginate was obtained from FMC BioPolymers (Drammen, Norway), and $CaCl_2$ was obtained from Sigma–Aldrich.

2.2. Preparation of cell-laden alginate solution

Alginate solution for dispensing was prepared using the technique and optimized processing conditions described in our previous work (Ahn et al., 2012a,b). The alginate was mixed with phosphate-buffered saline (PBS) to prepare 3.5 and 6 wt% alginate solutions. The 3.5 wt% alginate was used for the shell region in the core/shell strut and for a control scaffold. The 6 wt% alginate was used for the core region in the strut. To increase the viscosity of the solution before loading cells, the 3.5 wt% alginate was mixed with 0.5 wt% $CaCl_2$ at a 7:3 ratio. MC3T3-E1 cells were mixed with the 3.5 wt% alginate solution for a final density of 1.6×10^6 cells mL^{-1} using a three-way stopcock tool. The cell-alginate mixture was loaded into a syringe dispenser.

2.3. Fabrication of single alginate strut and 3D alginate scaffolds

A computer-controlled three-axis robot system (DTR2-2210T, Dongbu Robot, Bucheon, South Korea) coupled with a micro-syringe dispenser and an aerosol humidifier (Tess-7400; Paju, South Korea) was used to fabricate a single strut of cell-laden

Table 2
Processing parameters for various cell-laden alginate struts.

Fig. 3(a–f)	(a)	(b)	(c)	(d)	(e)	(f)
Pneumatic pressure (kPa)	220 ± 10	Core: 50 ± 6 Shell: 200 ± 22	Core: 100 ± 11 Shell: 200 ± 22	Core: 250 ± 28 Shell: 200 ± 22	Core: 270 ± 30 Shell:130 ± 14	Core: 100 ± 11 Shell: 180 ± 20
Strut size (μm)	857 ± 42	857 ± 42	914 ± 46	914 ± 46	806 ± 40	971 ± 49
Nozzle size (μm)	310	Core: 500, Shell: 900				Core: 500 Shell: 1070
Cells (number per mL)	1.6×10^6					

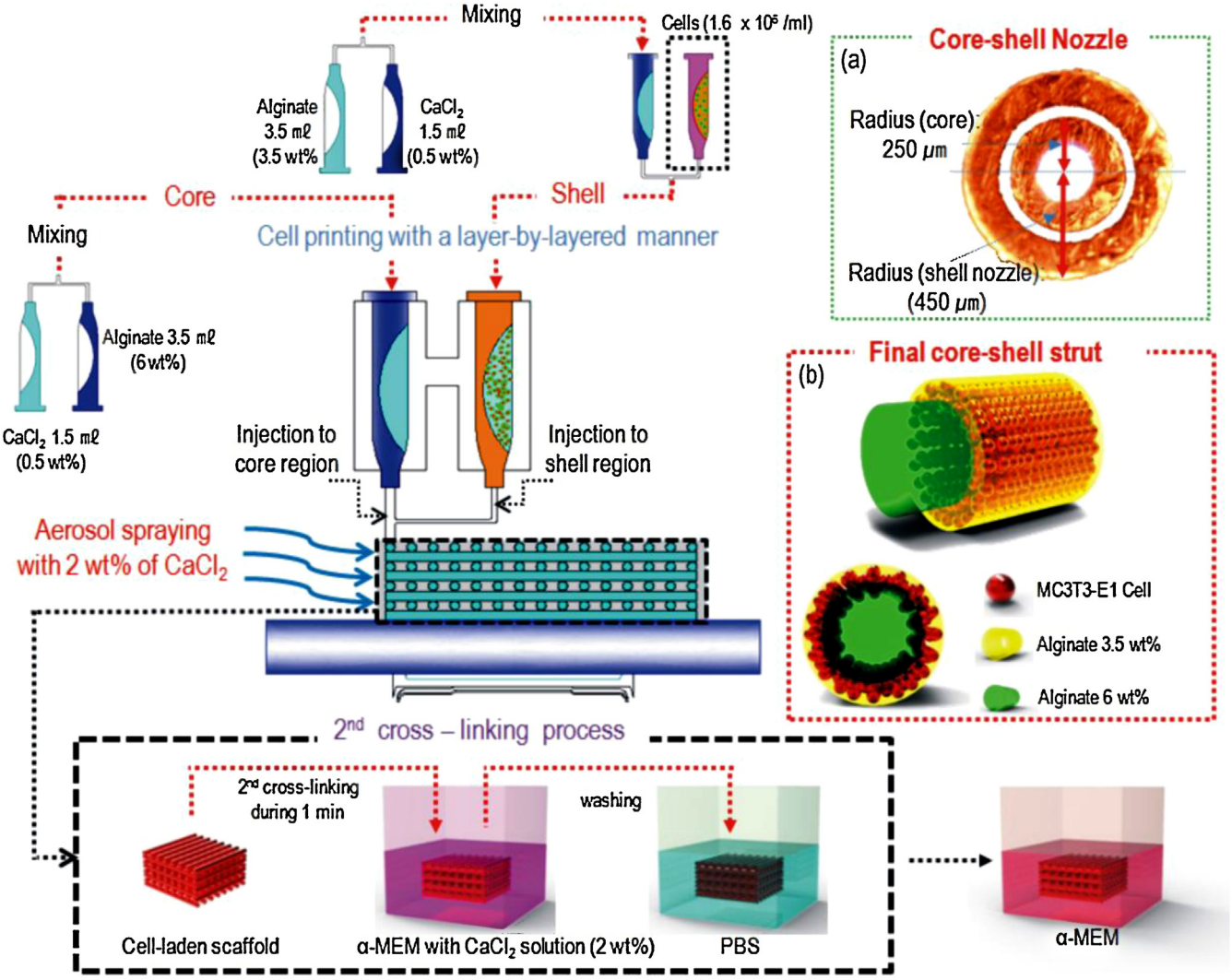

Fig. 1. Scaffold fabrication procedure with a three-axis robot dispensing system coupled to a micro-sized core/shell nozzle and an aerosol spraying process ($CaCl_2$ solution, 2 wt%). (a) Geometry of the cross-sectional core/shell nozzle and (b) the final core/shell strut, which consisted of the core region (6 wt% alginate without cells) and the shell region (mixture of 3.5 wt% alginate and cells, 1.6×10^6 mL^{-1}).

alginate and layer-by-layer cell-laden-alginate scaffold. Various pneumatic pressures were applied to the dispensing system to extrude the mixture of cells and alginate (Tables 1 and 2). The stand-off distance between the nozzle and working stage was 300 μm. In the aerosol spraying process, the rate of continuous $CaCl_2$ aerosol flow onto the dispensing stage was fixed at 1.5 ± 0.2 mL min^{-1}. Macroscopic and porous hydrogel scaffolds were fabricated as each alginate layer adhered to the previous one perpendicularly, forming a 0°/90° strut structure. After fabricating the multilayered alginate struts, the alginate scaffolds were again cross-linked with 2 wt% $CaCl_2$ solution for 1 min, which was optimized in our previous work (Ahn et al., 2012a,b).

2.4. Compression mechanical test

The cell-laden scaffolds were prepared with an 8-mm biopsy punch. The sample (thickness = 1.3 ± 0.5 mm) was submerged in PBS, most of the solution was removed, and the samples were loaded into a dynamic mechanical analyzer (DMA-Q800, TA-Instruments, USA) in controlled-force mode. The stress–strain curves for the scaffolds were recorded at a force ramp rate of 1 N min^{-1} and preload force of 0.001 N. The slope of the linear portion of each plot was calculated to determine the tangent Young's modulus ($n = 5$).

2.5. Cell viability measurements

Cell-laden structures (single strut and 3D scaffold) were exposed to 0.15 mM calcein AM and 2 mM ethidium homodimer-1 for 45 min in an incubator. The stained structures were observed under a microscope (TE2000-S; Nikon, Tokyo, Japan) equipped with an epifluorescence attachment and a SPOT RT digital camera (SPOT Imaging Solutions, Sterling Heights, MI, USA). To evaluate cell viability, we captured the images and processed the number of green and red spots using the Image-J program (NIH, Bethesda, MD, USA). The ratio of the number of live cells to the total number of cells (live and dead) was calculated using the software, and the ratio was normalized to the initial cell viability, which was the value prior to cell-alginate extrusion. The initial viability was determined using trypan blue (Mediatech, Herndon, VA, USA).

2.6. In vitro cell culture

Cell-laden structures (single strut and 3D scaffolds) were cultured and maintained in α-minimum essential medium containing

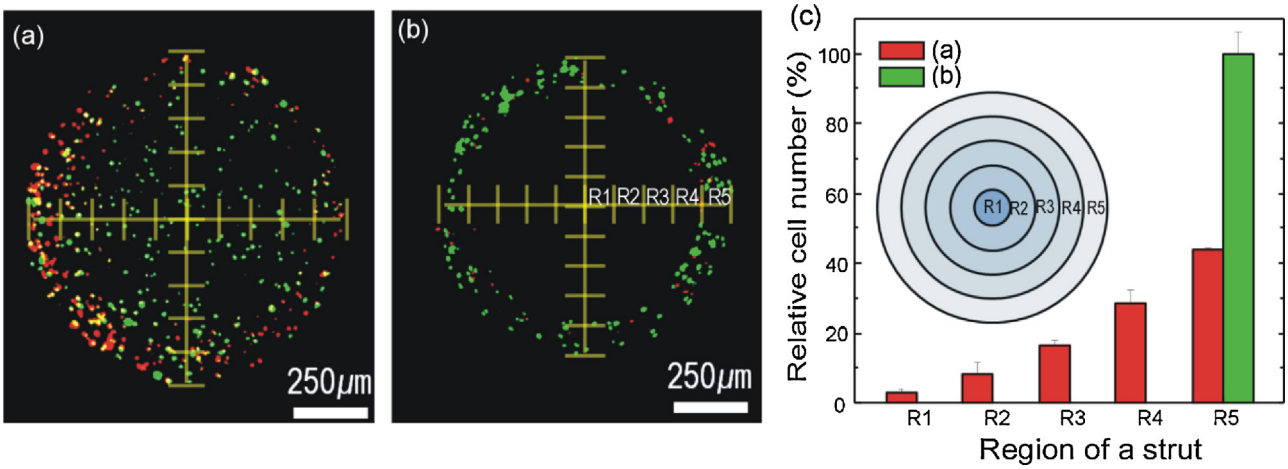

Fig. 2. Cross-sectional fluorescence images (live: green; dead: red) for (a) the control alginate strut and (b) the strut having core (without cells, 6 wt% alginate) and shell regions (cells and 3.5 wt% alginate). (c) Relative cell numbers for various regions (R1, R2, R3, R4, and R5) of the cross-sections of the single strut, indicating cell distribution in the axial direction of the strut. (For interpretation of the references to color in this figure legend, the reader is referred to the web version of this article.)

10% FBS and 1% antibiotics (antimycotic; Cellgro, Mediatech, Manassas, VA). The structures were incubated in an atmosphere of 5% CO_2 at 37 °C, and the medium was changed every second day. After 20 days of cell culture, the cell-laden scaffolds were analyzed with diamidino-2-phenylindole (DAPI) fluorescent stain to characterize the nuclei of the cells in the scaffold. Phalloidin (Invitrogen Inc., USA) was used to visualize the actin cytoskeletons of proliferated cells in the scaffolds.

3. Results and discussion

In cell-laden hydrogels, nutrient diffusion, waste removal, and oxygen transport between the entrapped cells and the surrounding environmental are key factors that affect cell survival. To achieve high cell viability after long cell-culture periods, the thickness of the cell-embedded hydrogels should be reduced for efficient diffusion of nutrients to the laden cells; according to Fick's second law, diffusion can be highly dependent on the hydrogel thickness. In most hydrogels, the primary mechanism for nutrient transport is diffusion, not convection (Slaughter, Khurshid, Fisher, Khademhosseini, & Peppas, 2009). Several studies have shown that reducing the hydrogel thickness can increase the viability of the embedded cells (Cruise et al., 1999; Chang, Nam, & Sun, 2008).

Fig. 1 shows a schematic diagram of our fabrication process, including the geometry of the core/shell nozzle [Fig. 1(a)] and the fabricated core/shell struts [Fig. 1(b)]. The core region was occupied by a high weight fraction (6 wt%) of alginate to improve the mechanical properties of the cell-laden scaffold, while cells in the shell region were injected with a mixture of 3.5 wt% alginate solution to improve cell viability during long cell-culture periods. In this work, we designed the pore and strut size of the cell-laden scaffolds to be 750 μm. However, during the extrusion process, the alginate solution experienced extrudate swelling; thus, we could not obtain the desired pore and strut size. The processing conditions and the measured pore and strut sizes are listed in Table 1. The concentration of cells injected into the struts was constant under all processing conditions, 1.6×10^6 mL^{-1}. As a control, cells were injected into the alginate scaffold (3.5 wt%) having similar pore and strut sizes to obtain a uniform axial distribution of cells in the struts.

Fig. 2(a) shows the cross-sectional fluorescence image of the strut fabricated with a single nozzle (310 μm), which exhibited homogeneous axial distribution of cells. Fig. 2(b) shows the cross-sectional image of the core/shell strut fabricated using a core/shell nozzle, which exhibited a high concentration of cells in the shell region. Details of the processing conditions are provided in Table 1. In the fluorescence images, the green and red colors indicate live and dead cells, respectively. As shown in the image of Fig. 2(b), the core/shell structure of the alginate strut was successfully fabricated, and most cells resided in the shell region. Sufficient nutrient transport and waste removal require a maximum cell-block thickness of 100 μm (Haraguchi et al., 2012); therefore, we set the shell region (i.e., thickness of the cell-laden area in the strut) to be 100 μm thick. The cell distributions in several cross-sectional regions (R1, R2, R3, R4, and R5) of the strut were compared by measuring the relative cell density (number of cells in each region/total number of cells) in the regions. As shown in Fig. 2(c), the cell distributions were well controlled for the homogeneously distributed cells (standard cell-laden strut) and for the cells concentrated in the shell region (R5) of the strut.

To verify the feasibility of the core/shell approach, we fabricated several struts by changing the applied pressures in the core and shell regions. The core consisted of 6 wt% alginate without cells, and the shell consisted of a mixture of cells (1.6×10^6 mL^{-1}) and 3.5 wt% alginate. To observe the distribution of the laden cells in the core/shell region, we sampled live cells from the various core/shell struts. Fig. 3(a) shows the standard cell-dispensing process using the single nozzle for the mixture of cells and 3.5 wt% alginate. Fig. 3(b)–(e) shows the core/shell struts fabricated using various extrusion pressures in the core/shell nozzle. Fig. 3(f) shows another technique used to design a half-moon structure in which half of the area contains a high weight fraction (6 wt%) of pure alginate and the other half contains the cell-laden alginate component; this structure was achieved by controlling the position of the center nozzle of the core/shell nozzle. Fig. 3(g) shows the relative area of the core region (A_c/A_T) for various pressure ratios (P_c/P_s) in the core/shell nozzle, where A_c and A_T are the area of the core and the total area of the cross-section of the strut, respectively. P_c is the extrusion pressure of the core nozzle, and P_s is the pressure of the shell nozzle. The core area of the strut increased linearly with increasing applied pressure ratio, indicating that the core area can be easily controlled by varying the pressure of the core nozzle. Details of the fabrication conditions are provided in Table 2.

Our previous work showed that the highly porous cell-laden scaffolds had significantly improved cell viability, but poor mechanical properties (decrease 45% of the compressive modulus compared to the non-porous scaffold) (Ahn et al., 2012a,b). The poor mechanical properties of the porous cell-laden scaffold was another motivation for the current work. As shown in Fig. 3(b)–(e), we obtained controlled core areas at the same weight fraction (6 wt%) in the single strut by varying the extrusion pressure.

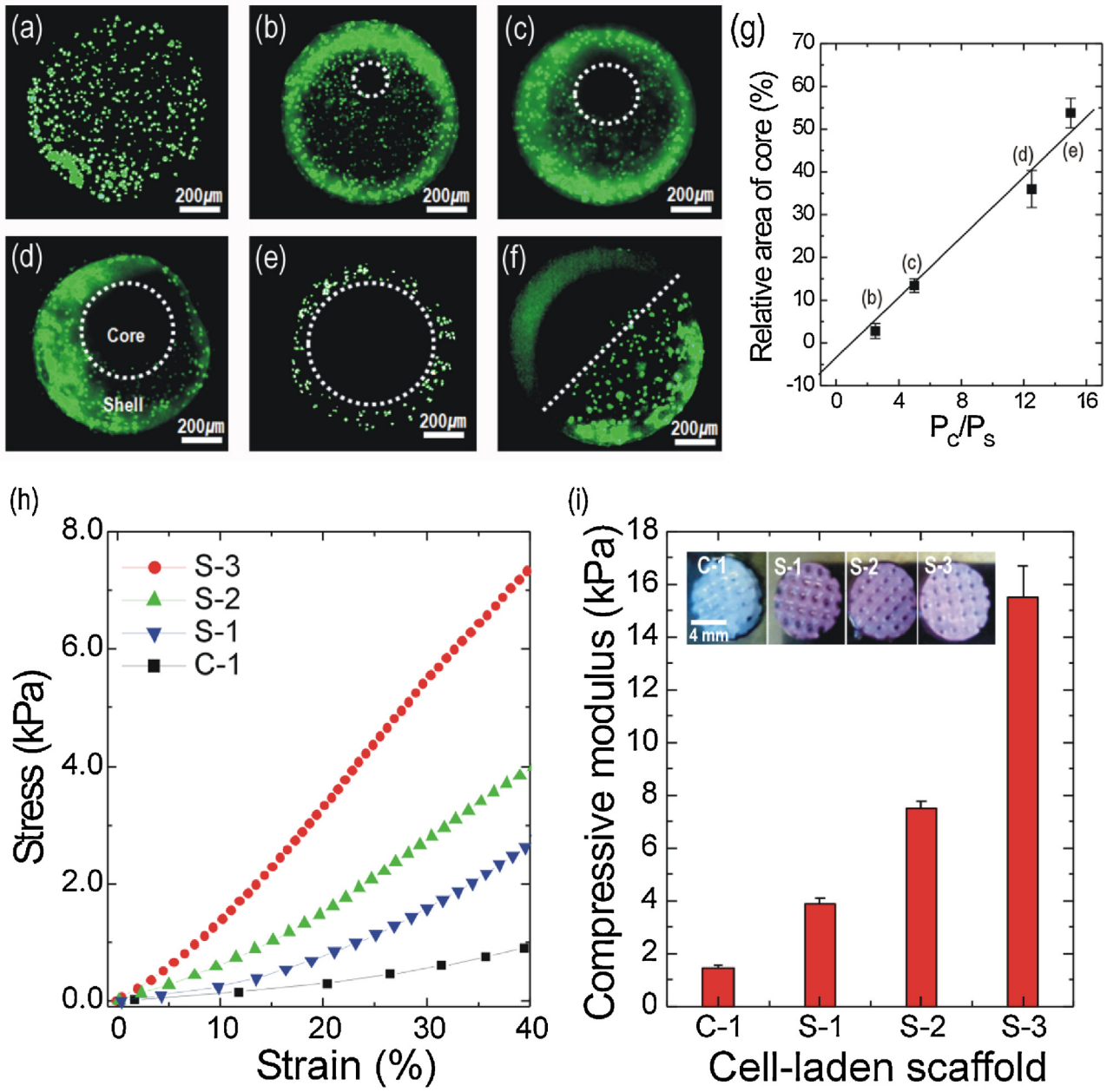

Fig. 3. Fluorescence images of the cross-sections of single struts showing the core/shell region. (a) Standard single strut with homogeneous cell distribution in the axial direction, (b–e) various struts with different core areas obtained by varying the extrusion pressure of the core/shell nozzle, and (f) a single strut having a half-moon structure. Green spots indicate live cells. (g) Relative area of the core region for various pressures used in the dispensing process, where P_C and P_S are the core pressure and shell pressure, respectively. (h) Stress–strain curves for various scaffolds and (i) compressive modulus values of the scaffolds. (For interpretation of the references to color in this figure legend, the reader is referred to the web version of this article.)

Compression tests were performed on the scaffolds to determine the effect of the reinforcing core region of 6 wt% alginate on the mechanical properties. In Fig. 3(h), C-1 is the scaffold fabricated using the standard cell-dispensing process (control); it consisted of the struts in Fig. 3(a). S-1, S-2, and S-3 are the scaffolds consisting of the struts in Fig. 3(c)–(e), respectively. The stress–strain curves for the cell-laden scaffolds are shown in Fig. 3(h). The Young's modulus (15.5 ± 1.2 kPa) of the core/shell scaffold (S-3) was significantly higher than that (1.4 ± 0.1 kPa) of the control alginate scaffold (C-1). Although both scaffolds had similar pore structures, the Young's modulus of the core/shell scaffold was greatly enhanced by the reinforcing core region. Additionally, the compressive modulus increased significantly with increasing core area, as shown in Fig. 3(i). This result suggests that if we vary the weight fraction of alginate in the core region of the scaffold, the mechanical properties of the cell-laden scaffold may be more controllable within a defined range.

Fig. 4(a) shows an optical image of the 3D cell-laden scaffold, which consisted of core/shell struts. The pore structure of the scaffold was well maintained, and the final fabricated size was about 20 mm × 20 mm × 4 mm. Fig. 4(b and c) shows optical images and live and dead cells for the control scaffold (C-1) and the core/shell scaffold (S-3) after 10 days of cell culture, respectively. For both scaffolds, the 3D pore structures, including pores and their interconnected channels extending continuously from top to bottom, were well maintained. However, the fluorescence images show that the control scaffold had much larger red spots (dead cells) than the core/shell scaffold; this phenomenon was similar on the surface and

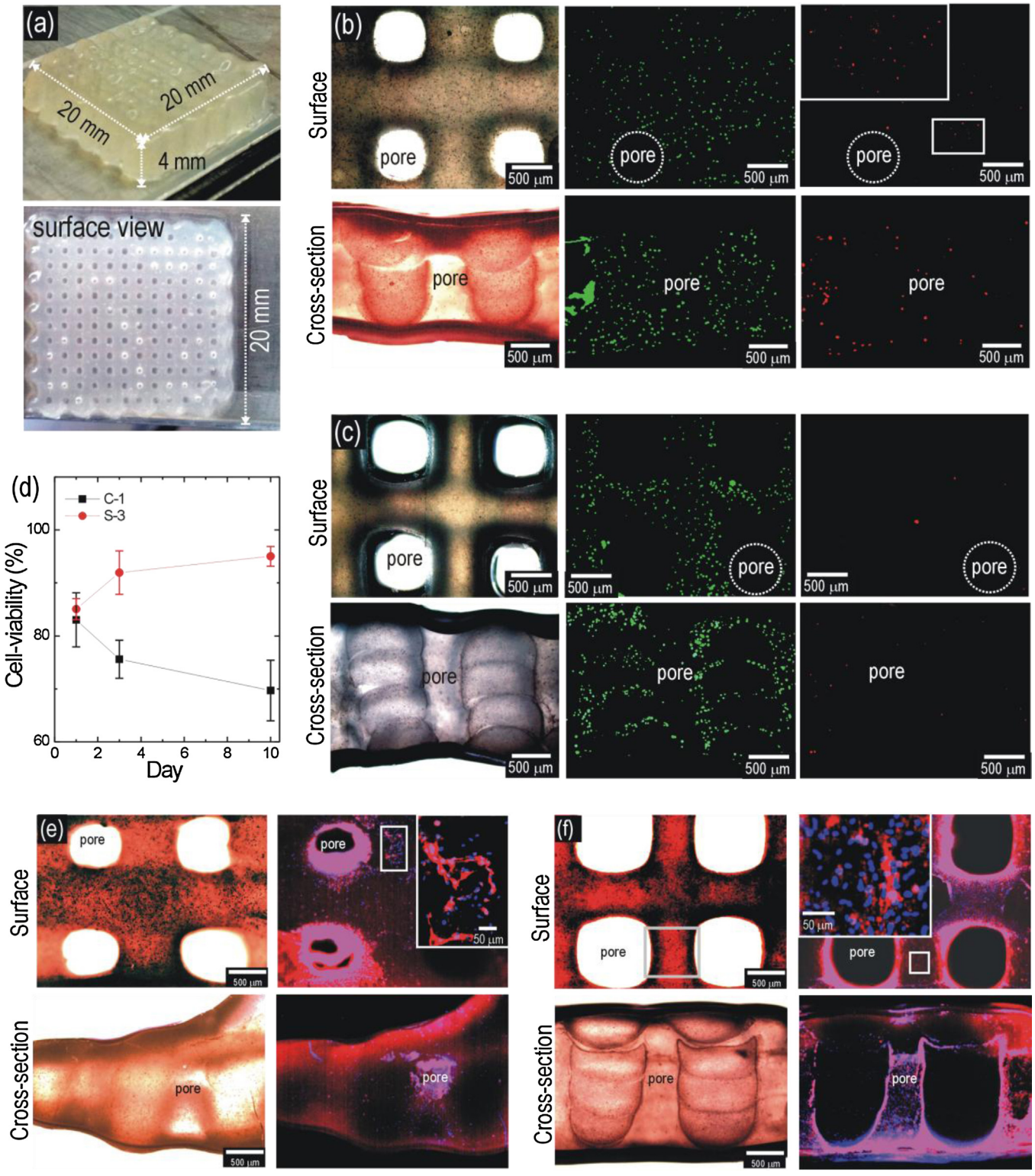

Fig. 4. (a) Optical images showing the fabricated core/shell scaffold with a size of 20 mm × 20 mm × 4 mm. Optical and fluorescence images showing live and dead cells after 10 days of cell culture for (b) C-1 and (c) S-3 scaffolds. (d) Cell viability for various cell-culture periods (1, 3, and 10 days) for C-1 (control) and S-3 (core/shell scaffold). Fluorescence surface and cross-sectional images of the scaffolds ((e) C-1 and (f) S-3) after 20 days of cell culture. Nucleus (blue) and F-actin (red). (For interpretation of the references to color in this figure legend, the reader is referred to the web version of this article.)

cross-sectional regions of the scaffolds. To determine the cell viability for both scaffolds after 1, 3, and 10 days of cell culture, the cell viability on the surface and cross-sectional areas were averaged. Fig. 4(d) shows the measured cell viability after various cell-culture periods. As the cell-culture period increased, the cell viability of the core/shell alginate scaffold became significantly higher than that of the control scaffold, although their cell viabilities at 1 day were similar. Thus, in the control scaffold, the cells in the core region of the struts gradually died due to low diffusion of nutrients, decreasing the final cell viability. However, in the core/shell scaffold, most cells

resided in the shell region, allowing nutrients to easily diffuse into the cells.

Fig. 4(e and f) show optical images of the stained nuclei (blue) and F-actin (red) in the scaffolds after 20 days of cell culture for the control and core/shell scaffolds, respectively. For both scaffolds, the laden cells actively proliferated on the alginate strut surfaces, but the cross-sectional views of the core/shell scaffold showed enhanced cellular activity over the entire region compared to the control scaffold. This result is attributed to the mechanical sustainability during long cell-culture periods. The pore structure of the core/shell scaffolds was well maintained because of the mechanically reinforced core region, while the control scaffold could not fully support its pore structure due to poor mechanical properties. Additionally, the laden cells in the core/shell scaffold effectively received nutrients and exchanged metabolic wastes because they resided in the shell region (less than 100 μm thick).

4. Conclusion

We reported a new cell-printing process, in which the distribution of cells in the scaffold was easily controlled using a core/shell micro-nozzle. The fabrication was performed using a three-axis robot system and an aerosol spraying method. By adjusting each nozzle pressure, we successfully obtained unique core/shell structures, in which the shell region was fully occupied by cells, and the scaffold showed significantly high cell viability (greater than 90% after 10 days of cell culture). We were able to control the mechanical properties of the fabricated cell-laden porous scaffolds by reinforcing the core region with a high weight fraction of alginate and varying core area. The functional 3D cell-laden hydrogel scaffolds with highly porous structures have great potential for applications in bottom-up tissue regeneration.

Acknowledgments

GH Kim is grateful to Prof. L. Bonassar for his permission for using various facilities in his laboratory of the Cornell University. This research was financially supported by the National Research Foundation of Korea Grant funded by the Ministry of Education, Science, and Technology (MEST) (Grant no. NRF-2012R1A2A2A01017435) and also was partially supported by a Grant of the Korean Health Technology R&D Project, Ministry of Health & Welfare, Republic of Korea (Grant no. A120942).

References

Ahn, S. H., Lee, H. J., Bonassar, L. J., & Kim, G. H. (2012). Cells (MC3T3-E1)-laden alginate scaffolds fabricated by a modified solid-freeform fabrication process supplemented with an aerosol spraying. *Biomacromolecules*, *13*, 2997–3003.

Ahn, S. H., Lee, H. J., Puetzer, J., Bonassar, L. J., & Kim, G. H. (2012). Fabrication of cell-laden three-dimensional alginate-scaffolds with an aerosol cross-linking process. *Journal of Materials Chemistry*, *22*, 18735–18740.

Atala, A., Bauer, S. B., Soker, S., Yoo, J. J., & Retik, A. B. (2006). Tissue-engineered autologous bladders for patients needing cystoplasty. *The Lancet*, *236*, 1241–1246.

Boland, T., Xu, T., Damon, B., & Cui, X. (2006). Application of inkjet printing to tissue engineering. *Biotechnology Journal*, *1*, 910–917.

Bruzewicz, D., Mcguigan, A. P., & Whitesides, G. M. (2008). Fabrication of a modular tissue construct in a microfluidic chip. *Lab on a Chip*, *8*, 663–671.

Catros, S., Guillemot, F., Nandakumar, A., Ziane, S., Moroni, L., Habibovic, P., et al. (2012). Layer-by-layer tissue microfabrication supports cell proliferation in vitro and in vivo. *Tissue Engineering Part C: Methods*, *18*, 62–70.

Chang, R., Nam, J., & Sun, W. (2008). Direct cell writing of 3D microorgan for in vitro pharmacokinetic model. *Journal of Tissue Engineering and Regenerative Medicine*, *14*, 157–166.

Cohen, D. L., Malone, E., Lipson, H., & Bonassar, L. J. (2006). Direct freeform fabrication of seeded hydrogels in arbitrary geometries. *Tissue Engineering*, *12*, 1325–1335.

Cruise, G. M., Hegre, O. D., Lamberti, F. V., Hager, S. R., Hill, R., Scharp, D. S., et al. (1999). In vitro and in vivo performance of porcine islets encapsulated in interfacially photopolymerized poly(ethylene glycol) diacrylate membranes. *Cell Transplantation*, *8*, 293–306.

Geckil, H., Xu, F., Zhang, X., Moon, S., & Demirci, U. (2010). Engineering hydrogels as extracellular matrix mimics. *Nanomedicine*, *5*, 469–484.

Gaetani, R., Doevendans, P. A., Metza, C. H. G., Alblas, J., Messina, E., Giacomello, A., et al. (2012). Cardiac tissue engineering using tissue printing technology and human cardiac progenitor cells. *Biomaterials*, *33*, 1782–1790.

Haraguchi, Y., Shimizu, T., Sasagawa, T., Sekine, H., Sakaguchi, K., Kikuchi, T., et al. (2012). Fabrication of functional three-dimensional tissues by stacking cell sheets in vitro. *Nature Protoccol*, *7*, 850–858.

Koch, L., Deiwick, A., Schlie, S., Michael, S., Gruene, M., Coger, V., et al. (2012). Skin tissue generation by laser cell printing. *Biotechnology and Bioengineering*, *190*, 1855–1863.

Langer, R., & Vacanti, J. P. (1993). Tissue engineering. *Science*, *260*, 920–926.

Matsunaga, Y. T., Morimoto, Y., & Takeuchi, S. (2011). Molding cell beads for rapid construction of macroscopic 3D tissue architecture. *Advanced Materials*, *23*, H90–H94.

Moutos, F. T., Freed, L. E., & Guilak, F. (2007). A biomimetic three-dimensional woven composite scaffold for functional tissue engineering of cartilage. *Nature Materials*, *6*, 162–167.

Ovsianikov, A., Deiwick, A., Van Vlierberghe, S., Dubruel, P., Moller, L., Drager, G., et al. (2011). Laser fabrication of three-dimensional CAD scaffold from photosensitive gelatin for applications in tissue engineering. *Biomacromolecules*, *12*, 851–858.

Slaughter, B. V., Khurshid, S. S., Fisher, O. Z., Khademhosseini, A., & Peppas, N. A. (2009). Hydrogels in regenerative medicine. *Advanced Materials*, *21*, 3307–3329.

Yang, J., Yamato, M., Sekine, H., Sekiya, S., Tsuda, Y., Ohashi, K., et al. (2009). Tissue engineering using laminar cellular assemblies. *Advanced Materials*, *21*, 3404–3409.